Supporting Information

Portable acoustic biosensing platform combined with paper-based capillary fluidics for the rapid detection of antibodies in serum

Dimitra Chronaki,[a] Stylianos Grammatikos,†[ba] Angelos Ntimtsas,†[a] Marios Matsis,[b] Orestis F. Kokolakis,[b] Konstantina Alexaki,[a] Zoi Pournara,[c] Achilleas Tsortos,[a] Alexandros Zafiropoulos[c] and Electra Gizeli*[ba]

[a] Institute of Molecular Biology and Biotechnology, Foundation for Research and Technology-Hellas, Heraklion, Crete 70013, Greece
[b] Department of Biology, University of Crete, Heraklion, Crete 70013, Greece
[c] Laboratory of Clinical Virology, Medical School, University of Crete, Heraklion, Crete 71003, Greece
†These authors contributed equally to this work

***Corresponding author**
E-mail: gizeli@imbb.forth.gr (E. Gizeli)

Keywords: surface acoustic wave (SAW) sensor; paper-based capillary fluidics; portable instrumentation; SARS-CoV-2; gold nanoparticles (AuNPs); point-of-care (POC) testing; immunoassay

Table of contents

TCD-AuNPs synthesis, bio-functionalization and characterization

Synthesis. TCD-AuNPs were synthesized using a modified Turkevich method, with TCD serving as both the reducing and stabilizing agent.[1] Briefly, 15 mL of an aqueous $HAuCl_4$ solution (1 mM) were heated to 95 ^oC. Subsequently, 1.5 mL of TCD (38.8 mM) were rapidly added to the heated solution under continuous stirring. The solution color changed from pale yellow to bluish-grey and finally wine red, indicating the successful formation of AuNPs. The reaction mixture was maintained under vigorous stirring and heating for a total of 20 mins, after which heating was discontinued and stirring continued until the solution reached room temperature (T_R). Finally, the suspension was stored at 4 ^oC until further use.

Bio-functionalization. To conjugate secondary antibodies to the AuNPs for use as signal amplification probes in the acoustic immunoassays, a passive adsorption protocol was employed. Initially, the TCD-AuNPs solution was appropriately diluted (three times, to ~4.78 nM) to achieve an optical density (OD) of 1. The solution was then centrifuged (4000 rcf, 20 mins) and redispersed in 2 mM of TCD with the pH adjusted to 9.0-9.5. Different amounts of secondary antibodies (10 - 1,000 nM) were incubated with the AuNPs solutions for ~1h. Afterwards, a salt stability test (addition of 10% w/v NaCl, equal volume) was performed to determine the optimal antibody concentration required for efficient surface coating of the AuNPs. The minimum concentration of goat anti-human IgG secondary antibody necessary to stabilize the AuNPs, was determined to be 1,000 nM. Finally, the final biofunctionalized AuNPs solutions used in the SAW acoustic immunoassays were centrifuged (13,000 rcf, 4 min) to remove the supernatant containing excess antibodies and subsequently resuspended to 0.1% w/v BSA in PBS (10 mM, pH = 7.4). A similar procedure was also followed for the QCM experiments used for the limit of detection (LoD) improvement estimation, with goat anti-rabbit IgG secondary antibody employed instead (minimum required concentration: 500 nM).

Characterization. In addition to their characteristic red color, the formation of TCD-AuNPs was confirmed by observing their surface plasmon resonance (SPR) band using UV-Visible absorption spectroscopy (Nanodrop One), with a cuvette. The TCD-AuNPs exhibited a UV-Vis absorption maximum at 522 nm with a narrow full width at half maximum (FWHM), indicating well dispersed AuNPs with an average diameter of ~13 nm. Based on this estimated size, the calculated concentration of the synthesized TCD-AuNPs was ~14.33 nM.[1] UV-Vis spectroscopy was also employed to evaluate the salt stability test (in addition to the visual color change from red to purple upon AuNP aggregation), and to confirm the successful binding of secondary antibodies to the AuNP surface (Fig. S1A, B). This was evidenced by a red shift of the UV-Vis absorption peak from 522 to 527 nm (Fig. S1A). The size and morphology of TCD-AuNPs were further investigated using field emission gun-scanning electron microscopy (FEG-SEM, JSM-IT700HR, Jeol Ltd., Tokyo, Japan), operating at an accelerating voltage of 15 kV. Samples for SEM analysis were prepared by drop-casting diluted colloidal solutions onto chemically cleaned silica substrates and allowing them to dry under ambient conditions. SEM micrographs revealed that the synthesized TCD-AuNPs were spherical and exhibited good size uniformity (Fig. S1C). Transmission electron microscopy (JEM-2100, Jeol Ltf., Japan) operating at an accelerating voltage of 200 kV, Mag-150k was also employed to study the morphology of TCD-AuNPs. TEM images further confirmed their spherical morphology and were used for precise size determination using ImageJ software (Fig. S1D). Approximately 250 AuNPs were measured from different regions of the TEM grid after drop-casting diluted TCD-AuNPs and drying. An average particle diameter of 12.75 $\pm$ 1.09 nm was obtained, in agreement with the size estimation derived from the UV-Vis data (Fig. S1E).

Morphological characterization of the functionalized SAW electrode surface

The surface morphology of the SAW electrodes was investigated using SEM micrographs after each layer deposition. Samples for SEM analysis were prepared by sequentially drop-casting each material onto the surface, allowing them to dry under ambient conditions between each modification step. SEM images were obtained for the following surfaces: bare Au, Au/PLL, Au/PLL/Spike, Au/PLL/Spike/Casein, Au/PLL/Spike/Casein/Serum and Au/PLL/Spike/Casein/Serum/AuNPs-2Ab, enabling stepwise evaluation of the surface modification process. The observed changes in surface morphology after each functionalization step support the successful sequential assembly of the sensing interface.

Supporting Figures

Fig. S1. Spectroscopic and morphological characterization of synthesized TCD-AuNPs

UV-Vis absorption spectroscopy was used to confirm the successful synthesis of TCD-AuNPs and the binding of goat anti-human IgG secondary antibodies to their surface (Fig. S1A, B). The addition of 1,000 nM secondary antibody was required to obtain stable biofunctionalized AuNP complexes, as lower concentrations resulted in broader FWHM values and a pronounced red shift, indicative of nanoparticle aggregation. Morphological characterization of the TCD-AuNPs was performed using SEM (Fig. S1C) and TEM (Fig. S1D), while particle size analysis revealed an average diameter of 12.75 $\pm$ 1.09 nm (Fig. S1E).

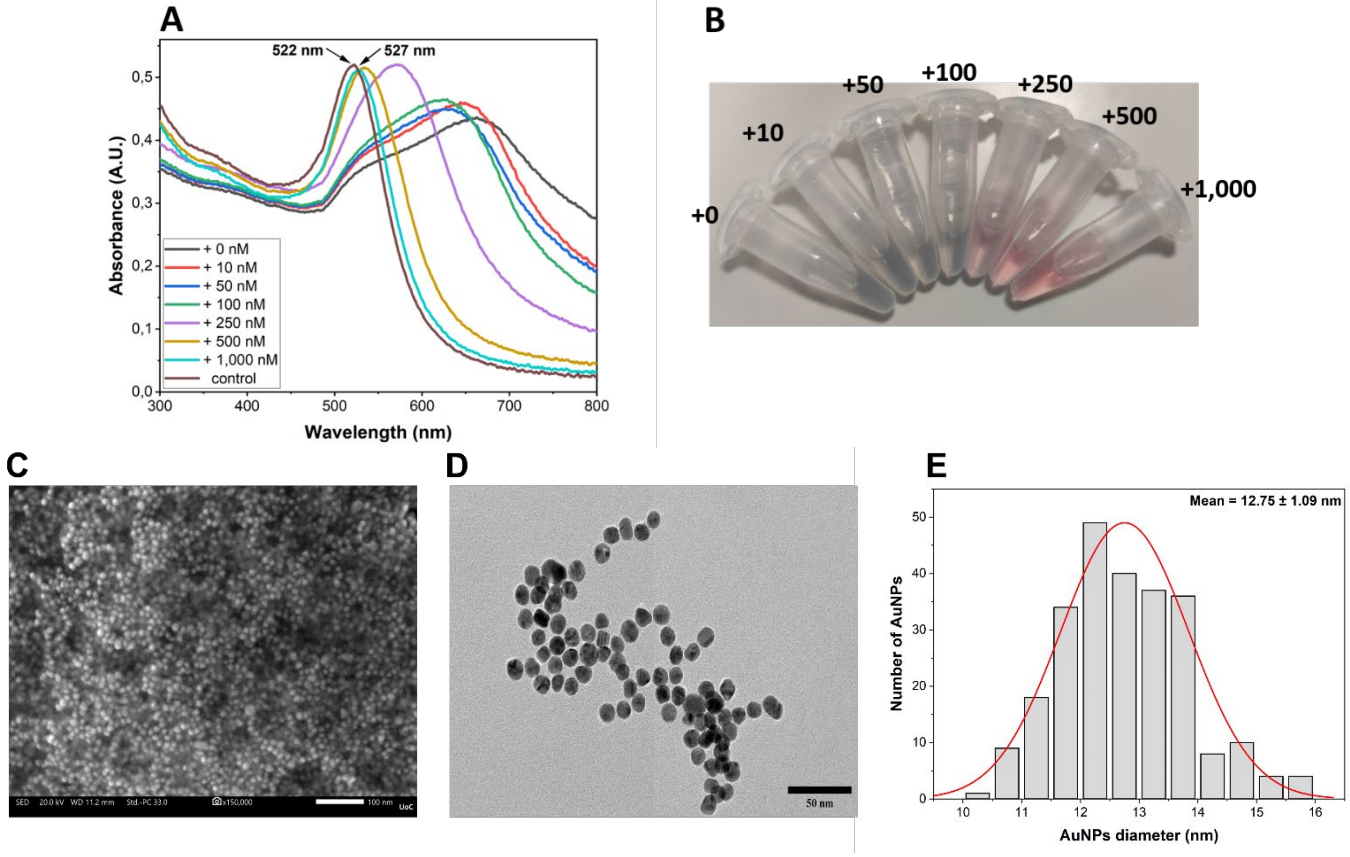

***Figure S1**: (A) UV-Vis absorption spectra of the synthesized TCD-AuNPs after incubation with different goat anti-human IgG secondary antibody concentrations and subsequent addition of 10% w/v NaCl. A concentration of 1,000 nM secondary antibody was required to obtain stable biofunctionalized AuNP complexes. Control measurement indicates TCD-AuNPs spectrum without NaCl addition. (B) Photograph of the tubes after NaCl addition, corresponding to the UV-Vis measurements. (C) Representative SEM image of TCD-AuNPs, demonstrating good uniformity in size and shape. Scale bar: 100 nm. (D) Representative TEM image of TCD-AuNPs, confirming their spherical morphology. Scale bar: 50 nm. (E) Size distribution histogram with a fitted distribution curve obtained from measurements of approximately 250 nanoparticles in TEM images acquired from multiple grid areas. TEM image analysis was performed using ImageJ software.*

Fig. S2. Average phase responses upon binding of human serum samples on Au/Spike/BSA vs. Au/PLL/Spike/Casein surface and control experiments

Twenty human serum samples were tested on both biorecognition surfaces and the phase signals are plotted below (Fig. S2A). The main categories of the tested human serum samples were: negative (< 3.16 RU/mL), low positive (11-116 RU/mL) and mild positive (140-530 RU/mL). As a general observation, the phase values in the PLL/Spike/Casein surface were drastically decreased compared to the Spike/BSA one. The low positive patients' sera were easily discriminated from the negative ones in both surfaces. In Spike/BSA, the average low positive signals were ΔPh = 0.523 ± 0.108 deg, while in PLL/Spike/Casein, the signals were ΔPh = 0.064 ± 0.019 deg (N = 6, for each). The average mild positive signals were ΔPh = 1.057 ± 0.260 deg in Spike/BSA and ΔPh = 0.376 ± 0.059 deg in PLL/Spike/Casein (N = 3, for each). Also, the non-specific binding of negative sera was minimized (ΔPh = 0.015 ± 0.029 deg) in PLL/Spike/Casein compared to Spike/BSA surface (ΔPh = 0.329 ± 0.033 deg) (N = 4, for each), probably due to the presence of casein blocker. BSA protein (67 kDa, ~7 nm) is widely used in ELISA but has been reported to allow some degree of non-specific binding in immunoassays.[2] On the other hand, casein which is a small protein (25 kDa, ~3 nm) has been effectively used as a blocker in immunoassays.[3,4] Due to its size, casein can fit and fill in surface gaps created after the antigen adsorption, while BSA will not fit due to steric hindrance.

The former was confirmed by a control experiment, in which a negative serum sample was added on PLL/BSA and PLL/Casein surfaces; indeed, negative serum bound non-specifically to BSA surface (ΔPh = 0.358 deg) while it was totally repelled by casein blocker (ΔPh = 0 deg) (Fig. S2B). This proves that the selected PLL/Spike/Casein immune-surface is better for discrimination among different serum titers. The higher phase signal upon Casein binding to PLL compared to BSA (Fig. S2B) has been also observed when these proteins adsorb directly on hydrophobic surfaces where BSA forms a compact monolayer (~7 nm) while casein forms multilayers (~7-8 nm).[5]

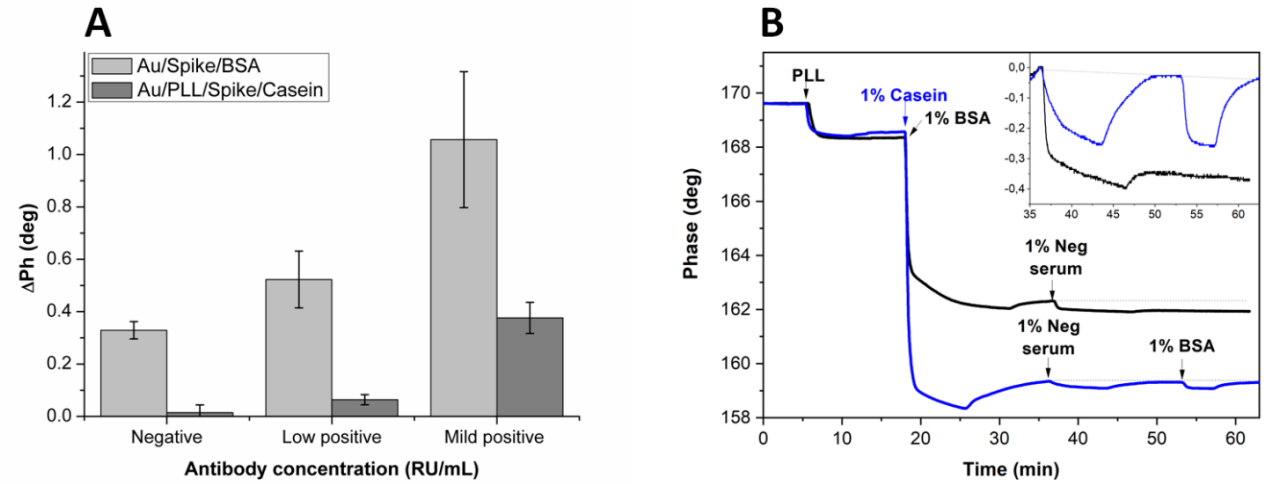

Figure S2: *(A) Phase signals obtained from human serum samples on the two biorecognition surfaces. The serum samples were categorized as negative (< 3.16 RU/mL), low positive (11-116 RU/mL) and mild positive (140-530 RU/mL). This graph shows a significant reduction in phase signals moving from Spike/BSA to PLL/Spike/Casein surface; especially, the non-specific binding of negative sera was minimized due to the presence of casein. (B) Phase signals upon binding of 1% v/v negative serum on PLL/BSA surface (black line) and on PLL/Casein surface (1% w/v BSA was added too) (blue line); zero non-specific binding of the negative serum is shown (magnified in the inset graph) in the presence of casein compared to BSA blocker.*

Fig. S3. Reproducibility study of biosensor performance using human serum samples on PLL/Spike/casein surface

To validate the reproducibility of the SAW biosensing performance, the optimized biorecognition surface (PLL/Spike/Casein) was utilized to bind anti-Spike antibodies from human serum samples. Three representative human serum samples (classified as low, mild and strong positive) were tested 10 times each, with the biosensor showing great reproducibility of the tested serum samples. The low positive patient (58.9 RU/mL) average signals were: ΔPh = 0.15 ± 0.03 deg and ΔA = 0.018 ± 0.002 dB, the mild positive (143.9 RU/mL) signals were: ΔPh = 0.47 ± 0.02 deg and ΔA = 0.049 ± 0.005 dB, while the strong positive (1043.4 RU/mL) signals were: ΔPh = 0.92 ± 0.12 deg and ΔA = 0.090 ± 0.009 dB.

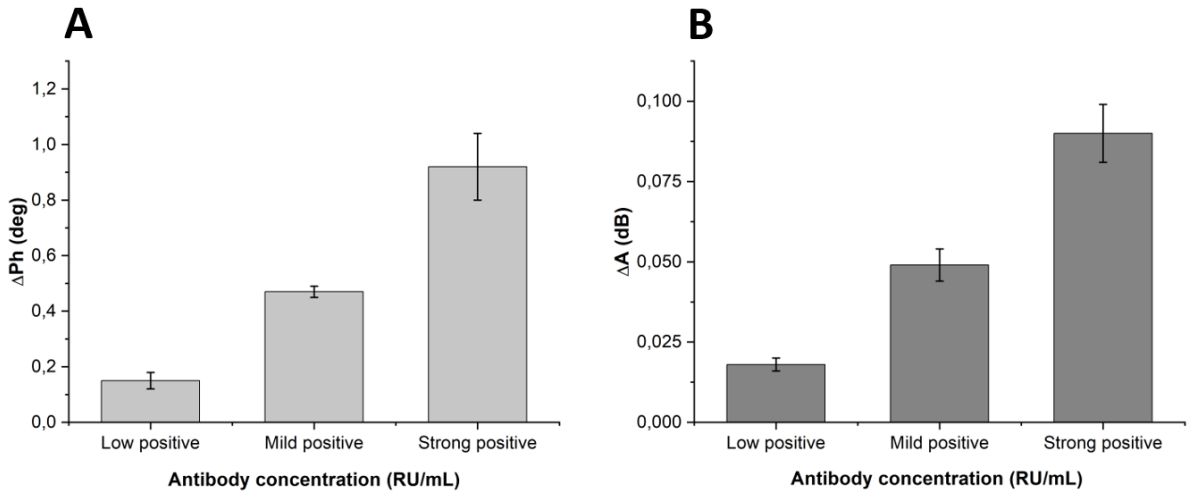

Figure S3: *(A) Phase and (B) amplitude signals obtained from human serum samples tested 10 times on the PLL-Spike-Casein surface. The 3 human serum samples used were low positive (58.9 RU/mL), mild positive (143.9 RU/mL) and strong positive (1043.4 RU/mL).*

Fig. S4. SEM micrographs obtained through the different modification steps of our optimized SAW electrode sensor surface

SEM images revealed a progressive change in surface morphology across each functionalization step, with an overall increase in apparent surface roughness and heterogeneity. The relatively uniform granular morphology of the bare Au surface becomes more diffuse following PLL coating, indicating the presence of a thin organic layer partially masking the underlying grains. Subsequent Spike protein immobilization further increases surface irregularity and reduces the visibility of grain boundaries, consistent with additional surface coverage. Similarly, casein blocking and serum exposure results in the appearance of larger clusters and aggregates, reflecting the adsorption of additional components. Finally, the presence of distinct bright dots of ~13 nm size in the AuNPs-modified surface, is consistent with the attachment of our functionalized AuNPs. It should be noted that these observations are qualitative, as no quantitative roughness analysis was performed.

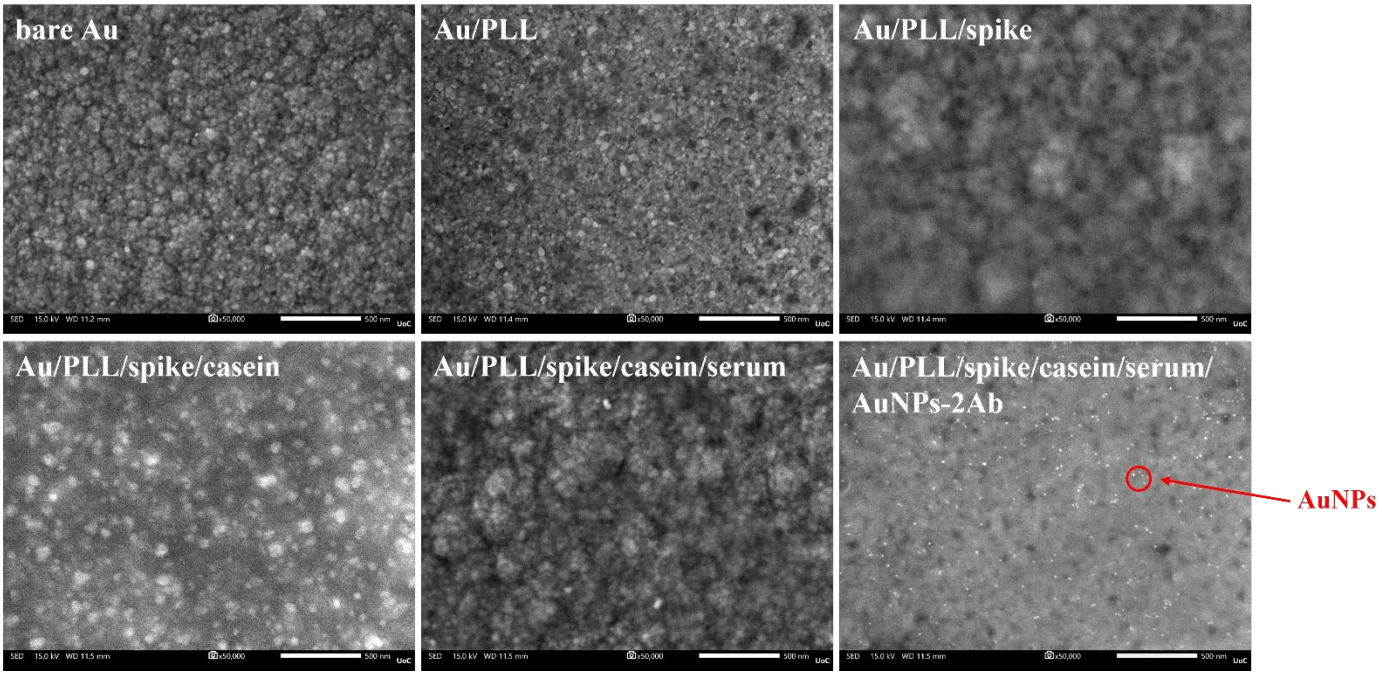

Figure S4: *SEM micrographs of the modified SAW electrode surface, following step-wise addition of each element. Distinct morphological differences between the different modified surfaces can be observed, indicating successful modification of the biosensing surface.*

Supporting Tables

Table S1. Phase and amplitude signals from PLL and Spike adsorption in the different set ups used

	(A) Spike on Au-SAW using commercial flow cell & benchtop instrument		(B) Spike on PLL-SAW using commercial flow cell & portable analyzer		(C) Spike on PLL-SAW using paper fluidics & portable analyzer	
	ΔPh (deg)	**ΔA (dB)**	**ΔPh (deg)**	**ΔA (dB)**	**ΔPh (deg)**	**ΔA (dB)**
PLL	---	---	1.02 ± 0.20	0.02 ± 0.01	2.02 ± 0.49	0.08 ± 0.04
Spike	10.87 ± 1.93	0.18 ± 0.03	7.34 ± 0.80	0.22 ± 0.04	5.92 ± 1.69	0.36 ± 0.15

Acoustic ratio$^{Spike\text{-}A}$ = 0.017 ± 0.004 dB/deg (N = 12)
Acoustic ratio$^{Spike\text{-}B}$ = 0.030 ± 0.004 dB/deg (N = 29)
Acoustic ratio$^{Spike\text{-}C}$ = 0.061 ± 0.010 dB/deg (N = 8)

Table S2. Phase and amplitude signals from 20 human serum samples tested on PLL layer using the commercial flow cell and portable measuring unit

	# of samples	**Direct**		**AuNPs**	
Serum sample		**ΔPh (deg)**	**ΔA (dB)**	**ΔPh (deg)**	**ΔA (dB)**
Negative (< 3.16 RU/mL)	4	0.015 ± 0.029	0.001 ± 0.002	0.013 ± 0.018	0.002 ± 0.002
Low positive (11-116 RU/mL)	8	0.088 ± 0.049	0.014 ± 0.006	0.155 ± 0.080	0.027 ± 0.011
Mild positive (140-530 RU/mL)	4	0.370 ± 0.050	0.033 ± 0.003	0.744 ± 0.157	0.099 ± 0.012
Strong positive (>1,000 RU/mL)	4	0.788 ± 0.246	0.072 ± 0.019	1.520 ± 0.124	0.214 ± 0.018

Table S3. Phase and amplitude signals from 3 human serum samples tested 10 times on PLL layer using the commercial flow cell and portable measuring unit

	# of repetitions	**Direct**	
Serum sample		**ΔPh (deg)**	**ΔA(dB)**
Low positive (58.9 RU/mL)	10	0.15 ± 0.03	0.018 ± 0.002
Mild positive (143.9 RU/mL)	10	0.47 ± 0.02	0.049 ± 0.005
Strong positive (1043.4 RU/mL)	10	0.92 ± 0.12	0.090 ± 0.009

Table S4. Phase and amplitude signals from 6 human serum samples tested on PLL layer using the capillary-based paper-fluidics

	# of samples	**Direct**		**AuNPs**	
Serum sample		**ΔPh (deg)**	**ΔA (dB)**	**ΔPh (deg)**	**ΔA (dB)**
Negative (< 3.16 RU/mL)	2	0.067 ± 0.025	0.008 ± 0.001	0.070 ± 0.056	0.018 ± 0.001
Low positive (40-90 RU/mL)	2	0.112 ± 0.020	0.021 ± 0.008	0.333 ± 0.093	0.064 ± 0.036
Mild positive (190-333 RU/mL)	2	0.361 ± 0.159	0.044 ± 0.013	1.457 ± 0.588	0.168 ± 0.076

Table S5. Representative comparison of biosensors for SARS-CoV-2 anti-Spike antibody (Ab) detection

Biosensor type	Detection Method	LoD	Sample type	Time-to-Result	Regenerability	PoC	REF
Love-SAW	Acoustic phase & amplitude change upon Ab binding	0.1 nM	Serum	< 30 min	Yes	High	This work
SH-SAW	Acoustic phase change upon Ab binding	41.8 BAU/mL	Whole blood	~40 s	No	High	6
Electrochemical	Current/impedance change upon Ab binding	0.3 fg/mL	Serum	~20 min	No	High	7
Nanoplasmonic	LSPR shift upon Ab binding	30 aM	Plasma	~15 min	No	Low-Moderate	8
Portable SPR	SPR shift upon Ab binding	~ ng/mL	Serum	< 30 min	Yes	Moderate	9
LFIA (colorimetric)	Colorimetric signal from NP-based immunoassay	5 ng/mL	Serum	~10 min	No	Very high	10
LFIA (fluorescent)	Fluorescence signal from NP-based immunoassay	0.1 ng/mL	Serum	~15 min (typical LFIA)	No	High	11
Optofluidic fluorescence	Fluorescence intensity change in microfluidic system	12.5 ng/mL	Serum	~25 min	No	Moderate-high	12
Transistor (OECT)	Gate voltage shift	10 fM	Saliva, serum	~5 min	No	High	13

As summarized above, although several platforms report ultralow limits of detection and rapid response times, they generally involve increased system complexity, labeling strategies, or lack true portability. In contrast, the proposed Love-SAW biosensor uniquely combines label-free operation (with optional AuNP-based signal amplification), real-time response, and surface regenerability within a compact and portable format. Furthermore, the integration of disposable paper-based capillary fluidics in place of conventional microfluidic systems, enables a cost-effective and simplified assay workflow, while maintaining rapid and quantitative antibody detection. This balanced combination of analytical performance and operational simplicity is not simultaneously achieved by the compared technologies, thereby underscoring the novelty of the present work.

Supporting References

1 W. Haiss, N. T. K. Thanh, J. Aveyard and D. G. Fernig, *Anal. Chem.*, 2007, **79**, 4215–4221.

2 H. I. Balcer, J. O. Spiker and K. A. Kang, *Adv. Exp. Med. Biol.*, 2003, **530**, 133–141.

3 C. H. Cheng, Y. C. Peng, S. M. Lin, H. Yatsuda, S. H. Liu, S. J. Liu, C. Y. Kuo and R. Y. L. Wang, *Biosensors (Basel).*, 2022, **12**, 2–11.

4 Y. C. Peng, C. H. Cheng, H. Yatsuda, S. H. Liu, S. J. Liu, T. Kogai, C. Y. Kuo and R. Y. L. Wang, *Diagnostics*, DOI:10.3390/diagnostics11101838.

5 L. Pérez-Fuentes, C. Drummond, J. Faraudo and D. Bastos-González, *Materials*, 2017, **10**, 893.

6 C.-H. Cheng, Y.-C. Peng, S.-M. Lin, H. Yatsuda, S.-H. Liu, S.-J. Liu, C.-Y. Kuo and R. Y. L. Wang, *Biosensors (Basel).*, 2022, **12**, 599.

7 Z. Rahmati, M. Roushani, H. Hosseini and H. Choobin, *Microchemical Journal*, 2021, **170**, 106718.

8 A. N. Masterson and R. Sardar, *ACS Appl. Mater. Interfaces*, 2022, **14**, 26517–26527.

9 A. Djaileb, M. Hojjat Jodaylami, J. Coutu, P. Ricard, M. Lamarre, L. Rochet, S. Cellier-Goetghebeur, D. Macaulay, B. Charron, É. Lavallée, V. Thibault, K. Stevenson, S. Forest, L. S. Live, N. Abonnenc, A. Guedon, P. Quessy, J.-F. Lemay, O. Farnós, A. Kamen, M. Stuible, C. Gervais, Y. Durocher, F. Cholette, C. Mesa, J. Kim, M.-P. Cayer, M.-J. de Grandmont, D. Brouard, S. Trottier, D. Boudreau, J. N. Pelletier and J.-F. Masson, *Analyst*, 2021, **146**, 4905–4917.

10 Z. Wang, Z. Zheng, H. Hu, Q. Zhou, W. Liu, X. Li, Z. Liu, Y. Wang and Y. Ma, *Lab Chip*, 2020, **20**, 4255–4261.

11 J. Ju, X. Zhang, L. Li, S. Regmi, G. Yang and S. Tang, *Front. Bioeng. Biotechnol.*, DOI:10.3389/fbioe.2022.1042926.

12 D. Song, J. Liu, W. Xu, X. Han, H. Wang, Y. Cheng, Y. Zhuo and F. Long, *Talanta*, 2021, **235**, 122800.

13 H. Liu, A. Yang, J. Song, N. Wang, P. Lam, Y. Li, H. K. Law and F. Yan, *Sci. Adv.*, DOI:10.1126/sciadv.abg8387.